Journal of Molecular Liquids 429 (2025) 127570

Contents lists available at ScienceDirect

Journal of Molecular Liquids

journal homepage: www.elsevier.com/locate/molliq

Anticancer effect of tamoxifen and Fe_3O_4@SiO_2@Cu hybrid NPs on malignant human breast cancer cell (MCF-7)

Sadegh Salimi [a], Gholamreza Motalleb [a,*], Hossein Dehghani [b], Abbas Rahdar [c,*], Kazem Dastjerdi [d,e], Brenda Velasco [f], Pablo Taboada [f,*]

[a] Division of Cell and Molecular Biology, Department of Biology, Faculty of Science, University of Zabol, Zabol, Islamic Republic of Iran
[b] Department of Molecular Medicine, School of Medicine, Birjand University of Medical Sciences, Birjand, Islamic Republic of Iran
[c] Department of Physics, University of Zabol, Zabol, Islamic Republic of Iran
[d] Cellular and Molecular Research Center, Birjand University of Medical Sciences, Birjand, Islamic Republic of Iran
[e] Department of Medical Biotechnology, Faculty of Medicine, Birjand University of Medical Sciences, Birjand, Islamic Republic of Iran
[f] Colloids and Polymers Physics Group, Particle Physics, Faculty of Physicst and Institute of Materials (IMATUS), Universidade de Santiago de Compostela 15782 Santiago de Compostela, Spain

ARTICLE INFO

Keywords:
Breast cancer
Fe_3O_4@SiO_2@Cu nanoparticles
Tamoxifen
Apoptosis
Oncogenes

ABSTRACT

This work examined whether co-administration of tamoxifen (TAM) and Fe_3O_4@SiO_2@Cu hybrid NPs to MCF-7 cancer cells may have an impact in cell cytotoxicity by increasing IC_{50} and apoptosis. NPs were produced using an electrochemical process and showed a negative surface charge (-35 ± 2 mV) and average hydrodynamic diameter and particle size of ca. 83 ± 1 nm and 60 ± 4 nm as derived from dynamic light scattering and electron microscopy images, respectively, and being colloidally stable in physiological conditions to long term. The particles were also shown to be non-toxic to cells in a wide range of concentrations. Notably, the co-administration of TAM (15 μg/mL) with Fe_3O_4@SiO_2@Cu nanocomposite (125 μg/mL) significantly reduced the IC_{50} of TAM from 15.1 μg/mL to 7.8 μg/mL ($P < 000.1$) after 72 h of incubation. Moreover, alterations in *p53*, *MDM2*, and *MDM4* gene expressions were determined using quantitative reverse-transcriptase polymerase chain reaction (qRT-PCR) directly related to the cell-death apoptotic pathway. The expression level of *p53* increased 2.1 times upon the co-administration of TAM with Fe_3O_4@SiO_2@Cu NPs nanoparticles compared with untreated MCF-7 cancer cells as the control group ($P < 0.001$); conversely, expression of *MDM2* and *MDM4* genes were 2.6 and 2.9 times lower compared to control cancerous cells ($P < 0.001$). On the other hand, fluorescence microscopy analysis showed that co-administration of TAM (15 μg/mL) with Fe_3O_4@SiO_2@Cu NPs (125 μg/mL) caused cell nuclei to break up. This was accompanied by changes in the cell shape, which proved that the nanoparticle-drug combination was highly cytostatic. Therefore, TAM co-administrated with Fe_3O_4@SiO_2@Cu NPs could be a promising and possible way to deliver TAM in breast cancer chemotherapy and enhanced its therapeutic effect.

1. Introduction

Cancer is quickly reaching cardiovascular diseases (CVDs) as the most prominent pathology in humans and is currently the second cause of mortality worldwide. By 2030, it is expected that 13 million people will die from cancer, and more than 21 million will be diagnosed with this disease [1]. Among them, over 2 million women were diagnosed with breast cancer (BC) in 2020 [2]. Breast cancer (BC) is a heterogeneous disease displaying different tumoral subtypes, luminal A, HER2-positive, triple-negative which display important genetic and structural differences with different cell populations within the proper tumor and its microenvironment, the so-called cancer heterogeneity, making difficult to find fully universal effective treatments for all patients, thus, leading to the need of developing more personalized therapies [3] to more effective treatments while avoiding drug resistances and unwanted adverse side effects [4]. What is clear is that poor prognosis and relatively high death rates are directly associated with such drug resistances after chemo and/or immunotherapies, the common standard of care nowadays for BC treatment [5]. Drug resistance mechanisms in BC are mainly associated, as in other types of cancer,

* Corresponding authors.
E-mail addresses: reza.motaleb@uoz.ac.ir (G. Motalleb), a.rahdar@uoz.ac.ir (A. Rahdar), pablo.taboada@usc.es (P. Taboada).

https://doi.org/10.1016/j.molliq.2025.127570
Received 19 November 2024; Received in revised form 11 March 2025; Accepted 8 April 2025
Available online 19 April 2025

with the expression and molecular activity of drug efflux pumps, pH changes in tumoral cells, inability to repair DNA damage, and methylation of different genes [6]. However, other mechanisms such as insensitivity to drug-induced apoptosis, drug-detoxification stimulation [7], and the expression of some oncogenes might also contribute to make chemo- and immunotherapies less effective [8].

On the other hand, the role of the *p53* gene has been extensively studied in recent years for its involvement in different types of cancer [9]. This gene plays a crucial role in regulating cellular growth and preventing the development of tumoral cells. The biological role of *p53* is as a tumor suppressor by detecting DNA damage and activating cellular repair [8]. However, mutations in this gene can lead to a loss of its function, allowing cells to divide uncontrollably and, thus, potentially leading to cancer development and progression. Preliminary studies have shown that genetic mutation and changes in the *p53* gene and *p53*-related signaling pathway (*p53*, *MDM2*, *MDM4*, *CDKN2A*, *CDKN2B*, and *TP53BP1*) are very common in BC, ca. 30 % of all cases [10]. In particular, BC is only one of few cancers in which the mouse double minute 2 (*MDM2*) and 4 (*MDM4)* genes are overexpressed or amplified. These genes are located at chromosome 12q14.3-q15 and chromosome 1 region q32, respectively, and seem to play key roles in tumor development and progression [10]. Particularly, MDM2, an E3 ubiquitin ligase, plays a crucial role in regulating the activity of the tumor suppressor *p53* in breast tissue [11], whereas *MDM4* inhibits *p53* by repressing its transcriptional activity and increase *p53* degradation when heterodimerized with MDM2 [12]. Therefore, understanding the role of the *p53* and directly related genes is crucial for BC treatment, making this signaling cascade a potential therapeutic target.

Tamoxifen (TAM) is an FDA-approved hydrophobic anticancer agent and selective estrogen modulator (SERM) for hormone-dependent BC, being one of the first line treatments of this type of cancer [13]. Despite its remarkable success, TAM dose-dependent carcinogenicity remains a concern, limiting its therapeutic uses [13]. Moreover, its efficacy can be also hindered by inherent developed drug resistance mechanisms after long periods of administration [14,15]. Currently, tamoxifen can be administered orally in the form of tablets or capsules for systemic administration [16]; topically, by direct application in the form of cream/gel to the breast skin for a more localized delivery; or by direct infusion using small tubes implanted near the tumor site, allowing for the sustained release of the drug directly to the surrounding cancer tissue [17]. The choice of the selected administration method depends on various factors, such as the type and stage of development of the tumor, dosage, treatment plan, and patient's preferences, amongst others.

However, these administration routes still have different drawbacks as, for example, the accumulation of suboptimal drug concentrations tumors, the existence of severe side effects, toxicity to healthy tissues and organs, etc. Thus, nanotechnology has become a prominent approach to address this problem, for example, by developing novel nanoformulations such as, for example, liposomes, micelles, polymeric nanoparticles (PNPs), solid lipid nanoparticles (SLNs), liquid crystalline nanoparticles (TAM-LCNPs), metallic nanoparticles (MNs), protein-based nanoparticles, and nano-lipid carriers (NLCs) to enable the local and targeted administration of this drug to malignant cells while prolonging the duration of treatment and reducing the overall used dose to prevent systemic toxicity [18] throughout the modification of both the pharmacokinetics and pharmacodynamics of the therapeutic cargo. Oppositely, the use of nanoparticles as nanovehicles can potentially hinder the prompt clearance of drugs from the body and subsequent accumulation in tissues and organs other than the targeted one. Hence, a potential alternative is to explore the enhancement of therapeutic activity of currently used bioactive compounds upon their coadministration with bioactive nanoparticles potentially bearing some coadjuvant and/or therapeutic effect with the objective of simultaneously affecting several pro-oncogenic pathways that could be concurrently active in tumor cells related to proliferation, migration, drug resistance, mutability, etc [19,20]. In this manner, coadministration can be more effective as it allows for a synergistic effect between the bioactive drugs producing a stronger therapeutic effect. For example, Keramati *et al.* [15] showed that the co-administration of 5-FU and gum-based cerium oxide NPs (CeO_2 NPs) significantly increased *p53*, *CASPASE-3*, *CASPASE-8* and *CASPASE-9* gene expressions compared to free administered 5-FU in human malignant colon carcinoma cells (Caco2). Van Vlerken et al. [21] reported that co-administration of paclitaxel and ceramide might be promising against multidrug resistance in the human ovarian cancer cell line SKOV3, whereas Deshpande et al. [22] reported an enhanced inhibition on smooth muscle cell proliferation. Stack *et al.* also showed that the biodistribution and tissue accumulation of targeted nanoparticles could be significantly enhanced by co-injection with polymeric micelles containing the actin depolymerizing agent latrunculin A by selectively inhibiting non-specific uptake of the second "effector" nanoparticle *in vitro* without impeding receptor-mediated endocytosis [23]. Moreover, different types of NPs as calcium phosphate, aluminium hydroxide and phosphate or silica have been shown to complementary stimulate the immune system to trigger an enhanced immune response upon vaccination [24,25].

In this regard, ferrite/iron oxide NPs and Fe_3O_4@SiO_2 core–shell NPs, which consist of a magnetite (Fe_3O_4) core and a silica (SiO_2) shell, have received great attention for biomedical applications as drug nanocarriers, imaging contrast and hyperthermia agents [26–28] and for their catalytic properties [29,30]. The silica shell surrounding the NPs provides further biocompatibility while ensuring their colloidal stability [31] by avoiding or decreasing the strong dipolar interaction between nanocores, which can lead to self-aggregation. Moreover, it can provide additional surface functional groups for the attachment or ligands or metals. The presence of Cu in the structure provides additional surface catalytical properties. In this regard, metallic copper and copper oxide NPs can induce oxidative stress; in particular, copper ions catalyze redox reactions, generating intracellular reactive oxygen species (ROS) like hydroxyl radicals through Fenton-like reactions and depleting glutathione [18]. This mechanism may selectively damage cancer cells, which are more sensitive to oxidative stress due to their high metabolic activity and low antioxidant capacity [32]. For example, Eisave *et al.* demonstrated that the incorporation of Cu on Fe_3O_4@SiO_2@PMA (being PMA phosphomolybdic acid) particles effectively catalyze the synthesis of several β-thiolo/benzyl-1,2,3-triazoles from various thiiranes, terminal alkynes and sodium azide very efficiently [33]. In addition, Darroudi et al. exploited the enhanced catalytic activity of Fe_3O_4@SiO_2@Cu NPs to provide a strong photo-catalytic effect able to be used to kill resistant bacteria [34].

Hence, in this study we aimed to evaluate whether a co-administration strategy of tamoxifen with catalytically-active Fe_3O_4@SiO_2@Cu hybrid NPs may have a direct impact in the whole antineoplastic effect of the drug. For such purpose, Fe_3O_4@SiO_2@Cu NPs were synthesized by means of an electrochemical method, and their size, morphology, surface charge, colloidal stability, composition and magnetic properties were analyzed using dynamic light scattering (DLS), transmission electron microscopy (TEM), laser Doppler anemometry, inductively coupling plasma-optical emission spectroscopy (ICP-OES), and vibrating sample magnetometry (VSM). Specifically, we aimed to assess whether this combination affects cell cytotoxicity of ER^+ MCF-7 BC cells *in vitro* by elevating the IC50 calculated by the MTT assay and decipher if cellular morphological alterations may take place as observed by fluorescence microscopy. Moreover, we also elucidated whether cell mortality might be related to alterations in gene expressions of *p53*, *MDM2* and *MDM4* genes, which are key regulators of the cell apoptotic pathway. For such purpose, the expression levels of these genes were quantified using qRT-PCR.

2. Materials and methods

2.1. Materials

Tamoxifen tablets (10 mg, chemical formula $C_{26}H_{29}NO$) were purchased from Tillomed Laboratories Ltd (UK). $FeSO_4{\cdot}7H_2O$, copper chloride, PBS, penicillin and streptomycin, DMSO and trypsin were from Sigma-Aldrich (USA). EDTA was from SinaClon (Iran); RealQ Plus 2 × Master Mix Green was purchased at Ampliqon (Denmark), fetal bovine serum (FBS) was from Gibco Invitrogen (USA), DMEM from PAN Biotech (USA) and MTT reagent from Acros Organic (USA), respectively. All material and reagents were of molecular grade.

2.2. Cell culture

Human malignant breast cancer cells (Michigan Cancer Foundation-7, ER^+/PR^+ $HER2^-$, ATCC MCF-7) were acquired from Pasteur Institute (Tehran, Iran). Cells were cultured in DMEM with 10 % FBS with 1 % (v/v) penicillin and streptomycin at 37 °C in 5 % CO_2, and 70–80 % humidity [35].

2.3. Preparation of Fe_3O_4@SiO_2@Cu hybrid NPs

Fe_3O_4 NPs were synthesized following an electrochemical method, in which a solution of iron (II) sulfate, under basic conditions, is induced to form nanoparticles on the surface of steel plates placed within a constant electric field, as previously reported [36]. Next, the SiO_2 shell coating was grown by dissolving 1 g of magnetite NPs in a mixed solution of 40 mL of ethanol and 10 mL of water and homogenize by ultrasounds. The solution was then transferred to a three-necked bottle and the pH s fixed at 10 using ammonia solution. A volume of 0.5 mL of tetraethyl orthosilicate was then added to the solution dropwise, and the resulting mixture stirred for 6 h at 50 °C. The NPs were then thoroughly washed with ethanol and distilled water and dried at 60 °C for 24 h [37]. Finally, a solution containing 0.90 g of copper chloride in 50 mL of 50 % (v/v) aqueous ethanol solution was added to a stirred mixture containing 0.27 g of Fe_3O_4@SiO_2 in 50 mL of 50 % (v/v) aqueous ethanol solution in an electrochemical cell. Then, over the course of 4 h and under reduced pressure, 1.6 mL of acetic acid and 8 mL of ethylene glycol were added dropwise. Afterwards, the obtained particles were then separated with a magnet, rinsed with deionized water, and calcined at 180 °C for 13 h to give Fe_3O_4@SiO_2@Cu NPs [37].

2.4. Particle characterization

The as obtained Fe_3O_4@SiO_2@Cu NPs nanoparticles were characterized using field emission scanning electron microscopy (FESEM) by Mira 3-XMU instrument capable of 700,000 × magnification (15.0 kV). Vibrating sample magnetometry (VSM) was carried out using a Kavir Precise magnetic instrument (MDKFT, Iran). Measurements were carried out at room temperature in a magnetic field of up to 8000 Oe. To characterize the hydrodynamic size of the particles an ALV-5000F static and dynamic light scattering system (ALV GmbH, Germany) equipped with a diode-pumped solid-state laser (2 W, Coherent Innova, USA) was used. Sizes were determined by means of the Stokes-Einstein relationship $r_h = k_BT/6\eta\pi D$, where T is the temperature, η is the viscosity of the continuous phase, D the diffusion coefficient, and k_B is the Boltzmann's constant. Inductively coupling plasma-optical emission spectroscopy (ICP-OES) was performed to account for the effective presence of Fe and Cu in the NPs through digestion of the NPs in aqua regia using a microwave digestion system. The digested solution was diluted with water and measured in an Agilent 5800.

2.5. Cell cytoxicity

Cell cytotoxicity of free TAM, bare Fe_3O_4@SiO_2@Cu NPs, and the coadministration of TAM with 125 μg/mL of Fe_3O_4@SiO_2@Cu NPs was evaluated using the MTT assay in MCF-7 cancer cells. Very briefly, 1 × 10^5 cells were added into each well of a 96-well plate, incubated for 24 h, and then cultured for 24 and 72 h in the presence of the different samples at different concentrations for cytotoxicity determination using the MTT assay, as reported by the manufacturer. The absorbance at 570 nm was measured using an Epon microplate reader (BioTek, USA). The cell survival rate (in %) was determined as follows:

$$\%\ survival\ rate = \left[\frac{Abs_{treated\ \ well\ \ (570\ \ nm)}}{Abs_{treated\ \ well\ \ (630\ \ nm)}} - \frac{Abs_{blank\ \ well\ \ (570\ \ nm)}}{Abs_{blank\ \ well\ \ (630\ \ nm)}} \Big/ \frac{Abs_{control\ \ well\ \ (570\ \ nm)}}{Abs_{control\ \ well\ \ (630\ \ nm)}}\right] \times 100 \quad (1)$$

The MLA_"Quest GraphTM IC50 Calculator" (AAT Bioquest, Inc., https://www.aatbio.com/tools/ic50-calculator) was used to determine the IC50 [38].

2.6. Hemocompatibility assessment

Freshly collected human blood samples from healthy volunteers were taken under consent agreement of donors. After three treatments with normal saline (0.9 % NaCl), red blood cells (RBCs) were separated by centrifugation at 3000 rpm for 10 min. Next, erythrocytes were washed several times until a transparent solution was achieved. Afterwards, the separated RBCs were further diluted with normal saline and then mixed again in PBS. The RBC solution was exposed to different NP concentrations followed by incubation at 37 °C for 2 h. After incubation, samples were subjected to another round of centrifugation at 3000 rpm for 15 min, and the resulting supernatant was collected for analysis. A microplate reader was used to measure the absorbance of the supernatant at 570 nm in order to determine the degree of hemolysis. PBS was used as the negative control and Triton X-100 (1 %) as the positive one. The extent of hemolysis was calculated as:

$$\begin{aligned}\%\ Hemolysis &= \frac{Abs_{sample} - Abs_{negative\ \ control}}{Abs_{positive\ \ control} - Abs_{negative\ \ control}} \times 100\%\ \text{Hemolysis} \\ &= \frac{\text{Abs (sample)} - \text{Abs (negative control)}}{\text{Abs (positive control)} - \text{Abs (negative control)}} \\ &\quad \times 100\%\ \text{Hemolysis} \\ &= \frac{\text{The sample} - \text{Negative control}}{\text{Positive control} - \text{Negative control}} \times 100\end{aligned} \quad (2)$$

2.7. Isolation of RNA and cDNA synthesis

Extraction of total RNA and cDNA synthesis were carried out according to the manufacturer's instructions using the Super RNA Extraction kit (AnaCell, Iran) and the cDNA Synthesis kit (AnaCell, Iran), respectively, according to the manufacturer's instructions. Briefly, prepared cell suspensions (<5 × 10^6 cells) were added to the lysing ethanol solution to prepare the RNA for column binding. Then, the obtained product was transferred to a silica column. Washing buffer was used to eliminate other chemicals from the column surface and released the pure

RNA. Purified RNA was then used for the synthesis of cDNA. First, the PCR master mix was incubated at 70 °C for 5 min and then suddenly cooled in ice. Afterwards, 6 μL of the mixture, comprising 4 μL of 5X RT buffer, 1 μL of dNTP mix, 0.5 μL of RNase inhibitor (RNAI), and 0.5 μL of M-MLV reverse transcriptase, were introduced. The anchored oligo (dT) primer was incubated at 42 °C for 60 min and subsequently at 70 °C for 5 s to inactivate enzymes.

2.8. Real-time quantitative reverse transcription polymerase chain reaction

The expression levels of *MDM2*, *MDM4*, and *p53* genes were evaluated using an Applied Biosystems StepOneTM Real-Time PCR System (Thermofisher Scientific, USA) and RealQ Plus 2x Master Mix Green (Ampliqon, Denmark) kit. Briefly, the synthesized cDNA was subjected to SYBER green real-time PCR. The *actin beta* (*ACTB*) gene was used as the housekeeping gene. The settings for quantitative reverse transcription PCR (qRT-PCR) are shown in Table 1. To measure the gene expression, the $2^{-\Delta\Delta Ct}$ method was used [13]. The Primer3 package was responsible for the automated creation of all primers [19]. Further primer specificity predictions were made with the help of the Primer-Blast web application.

2.9. Cell morphological evaluation by fluorescence microscopy

MCF-7 cells at a density of 5×10^5 were subjected to the different treatments at specific concentrations of TAM and Fe_3O_4@SiO_2@Cu NPs for 72 h. Cells were then collected and fixed in 80 % acetone at a temperature of 4C for 20 min. Subsequently, cell nuclei were stained with Hoechst 33,342 and incubated in darkness for 5 min, thereafter they were meticulously washed with phosphate-buffered saline (PBS). The potential induced morphological changes underwent by MCF-7 cells were observed through an inverted fluorescence microscope (Olympus IX70, Japan) at a magnification of 20X.

Table 1
Sequence of the primers designed for real time PCR assay.

Primer	Sequence (5′ → 3′)	Condition	Product size(bp)
MDM2: F	GCAGTGAATCTACAGGGACGC	95 °C for 15 min,	83
MDM2: R	ATCCTGATCCAACCAATCACC	40 Cycle: 95 °C for 15 s, 60 °C for 44 s Melt curve: 95 °C for 15 s, 60 °C for 1 min,	
MDM4: F	CTAAGTCCTTAAGTGATGATACCGATGT	95 °C for 15 min,	151
MDM4: R	AACTTTGAACAATCTGAATACCAATCC	40 Cycle: 95 °C for 15 s, 60 °C for 44 s Melt curve: 95 °C for 15 s, 60 °C for 1 min,	
p53: F	TGCGTGTGGAGTATTTGGATG	95 °C for 15 min,	90
p53: R	TGGTACAGTCAGAGCCAACCTC	40 Cycle: 95 °C for 15 s, 60 °C for 44 s Melt curve: 95 °C for 15 s, 60 °C for 1 min,	

Abbreviations
F = forward; R = reverse.

2.10. Ethical issues

This research was approved by University of Zabol and Birjand University of Medical Sciences with Ethics committee letter number Ir.bums.REC.1397.376 (1397/12/06).

2.11. Statistical analysis

The SPSS program (SPSS Inc., USA) v. 26 was used to analyze experimental data, and the findings were reported in terms of the mean and standard deviation. The assessment was conducted thrice independently. otherwise stated. One-way ANOVA (*P < 0.05; **P < 0.01; ***P < 0.001) was used to determine statistical differences for multiple groups, whereas unpaired *t*-test was used to analyzed individual groups.

3. Results

Fe_3O_4@SiO_2@Cu NPs were obtained using an electrochemical-based method. Fig. 1a show the hydrodynamic size distribution of the obtained NPs, with an average hydrodynamic diameter of ca. 83 ± 1 nm and an electric surface charge of −35 ± 2 mV. From FESEM images (Fig. 1b), Fe_3O_4@SiO_2@Cu NPs show an average particle size of ca. 60 ± 4 nm, in fair agreement with DLS data.

The colloidal stability of the nanoparticles was confirmed by the fact that the hydrodynamic diameter is almost maintained after prolonged incubation both in water and DMEM, in the latter medium thanks to the adsorption of the proteins present in the culture medium (see Fig. 1c). For the first 7 days of incubation, only very slight increases in hydrodynamic diameter of ca. 5 and 9 nm are observed for NPs in water and DMEM media, respectively, and which might be related to the presence of some isolated cluster upon dispersion; in the latter medium, DMEM, the adsorption of certain ligands present in the cell culture medium composition cannot be also disregarded; nevertheless, no evidence of either aggregation or precipitation even after 6 months of storage were noted, as observed by the naked eye (Fig. 1d). The magnetic characteristics of the particles were also assessed using a vibration sample magnetometer (VSM), revealing that have a very slight ferromagnetic behaviour at room temperature with a small finite coercivity of 30 Oe and a magnetic saturation of 55 emu/g as corresponds to this type of nanoparticles. The effective incorporation of Cu in the NPs was determined by ICP-OES, denoting a Fe:Cu ratio of ca. 5:1.

The therapeutic activity both free administered TAM and co-administrated with Fe_3O_4@SiO_2@Cu hybrid NPs were performed by the MTT assay in healthy mouse Balb/3T3 and human ER^+ positive MCF-7 breast cancer cells. Experimental data revealed a larger cellular toxicity of the hybrid NPs if compared with single TAM administration when exposed to MCF-7 cells but not in healthy ones (Fig. 2), probably as a consequence of the higher metabolic activity of the tumoral cells and internalization extents, as reported elsewhere [39]. As control, the nanoparticles were observed to be completely non-toxic below a concentration of 150 μg/mL. Moreover, the hemolytic activity of the Fe_3O_4@SiO_2@Cu hybrid NPs was also very reduced below 150 μg/mL (<2 %), in agreement with CCK-8 assay so that the materials can be considered as non-hemolytic according to standard ASTM F 756-08 [40].

On the other hand, for both cell lines the observed cytotoxicity was concentration-dependent. Half-maximal inhibitory concentrations (IC50) for Balb/3T3 and MCF-7 cells are shown in Table 2. In this Table, it can be observed that the co-administration of the drug with the Fe_3O_4@SiO_2@Cu hybrid NPs appears to increase the drug efficiency in

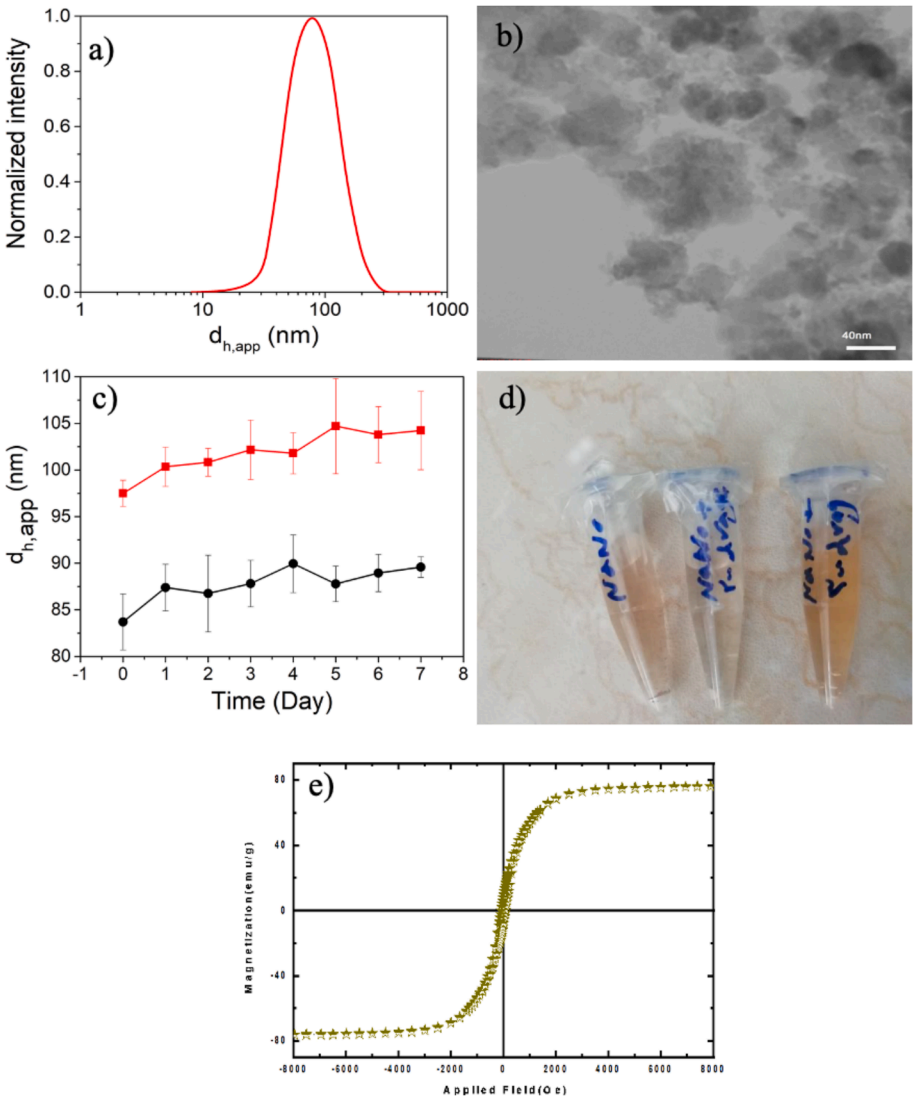

Fig. 1. a) Hydrodinamic size population distribution; b) FESEM image; c-d) colloidal stability in (●) water and (●) DMEM medium upon incubation; e) magnetic properties of of the obtained Fe_3O_4@SiO_2@Cu hybris NPs.

the tumoral cells as indicated by the reduction in IC_{50} values [19]; however, in healthy ones the variations are within the experimental uncertainty.

To analyze the potential origin of the detected cytotoxicity, changes in the expression levels of *MDM2*, *MDM4* and *p53* genes after the administration of the single drug (15 μg/mL) or co-administered with the NPs (125 μg/mL) were assessed by qRT-PCR, as shown in Fig. 3. Interestingly, the expression levels of *p53* increased 2.1 and 1.8 times for the TAM co-administrated with Fe_3O_4@SiO_2@Cu NPs-treated group compared with untreated and TAM-treated MCF-7 cancer cells as the controls, respectively. Conversely, *MDM2* and *MDM4* gene expressions were 2.6 and 2.9 times lower in MCF-7 cancer cells treated with TAM co-administrated with Fe_3O_4@SiO_2@Cu hybrid NPs compared with free TAM-treated MCF-7 cancer cells, respectively.

The potential morphological alterations in MCF-7 cancer cells after treatment with free TAM, bare Fe_3O_4@SiO_2@Cu hybrid NPs, and their combination (at the same concentrations utilized in gene expression experiments) were also evaluated using optical (Fig. 4a) and fluorescence microscopy (Fig. 4b). The untreated MCF-7 control group preserved cellular morphology characterized by distinct nuclei exhibiting intense blue fluorescence, as illustrated in Fig. 4a-i) and Fig. 4b-v, respectively.

Cancer cells treated with free TAM free exhibited nuclei fragmentation and condensation, as indicated by the red arrows in Fig. 4b-vi, although its extent was much lower than for the case of free TAM co-administered with the NPs (see below). The treatment with bare Fe_3O_4@SiO_2@Cu NPs did not induce notable morphological or nuclear alterations (Fig. 4a-iii; Fig. 4b-vii), confirming the inherent low cytotoxicity of the particle and biocompatibility at the selected dose. Conversely, important alterations in nuclei morphology were observed in MCF-7 cells in the presence of free TAM co-administrated with Fe_3O_4@SiO_2@Cu NPs (Fig. 4a-iv). In particular, cells underwent a transformation characterized by a loss of shape and a more rounded morphology with clear evidences of apoptosis, including chromatin, nuclear, and cytoplasmic condensation, much more intense than in the case of the free administered drug alone (Fig. 4b-viii). These alterations become even more pronounced along incubation (not shown), resulting in the separation of numerous cells and the formation of irregularly shaped clusters and a reduction in cell density occurred due to cellular detachment and mortality.

4. Discussion

The co-administration of two drugs/bioactive compounds to achieve

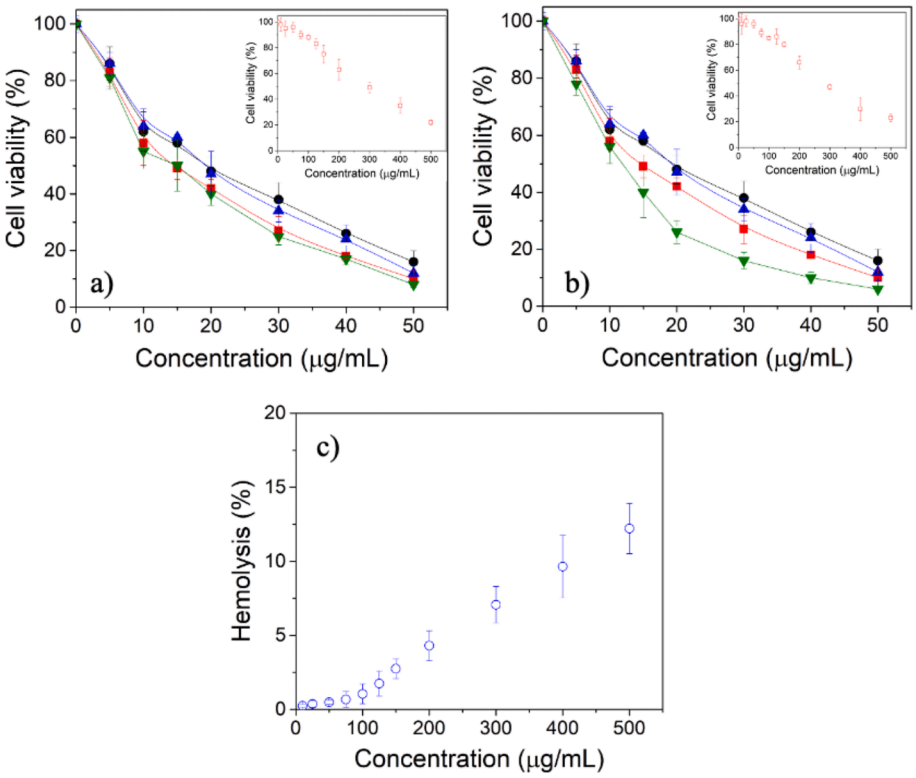

Fig. 2. Concentration-dependent cell cytotoxicity of (●,■) free TAM and (▲,▼) TAM co-administered with Fe_3O_4@SiO_2@Cu hybrid NPs after 24 and 72 h of incubation in a) mouse Balb/3T3 and b) human MCF-7 cells. The inset denotes the cytotoxicity of (○) bare NPs after 24 h of incubation. c) Hemolytic effect of Fe_3O_4@SiO_2@Cu hybrid NPs at different concentrations.

Table 2
IC50 values of free TAM, free Fe_3O_4@SiO_2@Cu NPs, and TAM co-administered with Fe_3O_4@SiO_2@Cu NPs after incubation with mouse Balb/3T3 and MCF-7 cells.

	Balb/3T3		MCF-7	
	24 h	72 h	24 h	72 h
Free TAM	19.5 ± 2.1	14.4 ± 1.8	20.7 ± 1.5	15.1 ± 1.1
Free NPs	278 ± 8.3	–	269 ± 7.8	–
TAM + NPs	19.2 ± 1.1	14.8 ± 1.3	17.0 ± 1.3	7.8 ± 0.9

a desired therapeutic goal is a widely used strategy in clinical practice to optimize treatments and achieve enhanced therapeutic efficacies [31]. Thus, the objective of this research was to enhance the anticancer properties of tamoxifen (TAM) through its co-administration with Fe_3O_4@SiO_2@Cu NPs, thereby creating a new therapeutic approach for the treatment of malignant human breast cancer cells (MCF-7).

Following this approach, in the present study we analyzed the therapeutic activity of the coadministration of TAM with Fe_3O_4@SiO_2@Cu nanocomposite, since these nanoparticles have been shown to possess potential beneficial properties as biocompatibility, colloidal stability, catalytic activity through Fenton-like reactions, and bioimaging and magnetic hyperthermia capabilities [31–33]. The synthesized Fe_3O_4@SiO_2@Cu NPs displayed spherical shapes and a consistent population size distribution, with mean particle sizes and hydrodynamic diameters of ca. 60 ± 4 nm and 83 ± 1 nm as derived by FESEM and DLS, respectively. Particles appear certainly aggregated in FESEM images as consequence of the inherent drying process required for sample preparation and visualization. Moreover, the observed larger hydrodynamic size obtained compared to particle size obtained by FESEM image analysis can be directly related to the entity which is inherently measured by DLS, that is, the NP core plus the bonded water solvent shell [41,42]; however, the existence of some particle clusters in solution cannot be disregard in spite of the elevated surface charge of the NPs, 35 ± 2 mV, which should be sufficient to electrically stabilized the particles. This is further corroborated when analyzing the particle stability. Hybrid NPs were colloidally stable in different physiologically-relevant media with no evidence of either aggregation or precipitation in solution even after 6 months of storage, as observed by the naked eye.

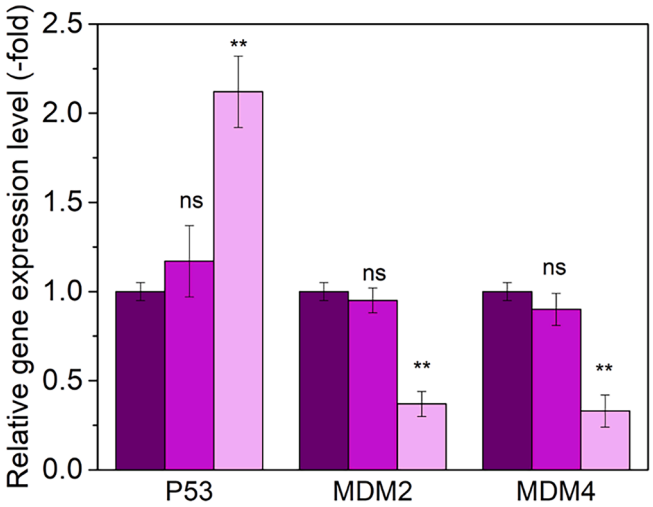

Fig. 3. Expression levels of *p53* (P = 0.001), *MDM2* (P = 0.001), and *MDM4* (**P = 0.01) genes in MCF-7 cancer cells (■) in the absence of treatment and treated with (■) only TAM (15 μm/mL) and (■) TAM (15 μm/mL) co-administered with 125 μm/mL of Fe_3O_4@SiO_2@Cu hybrid NPs. Data are expressed as mean value ± SD.

On the other hand, it was noted that the hybrid NPs were non-toxic and non-hemolytic to cells below a concentration of 150 μg/mL.

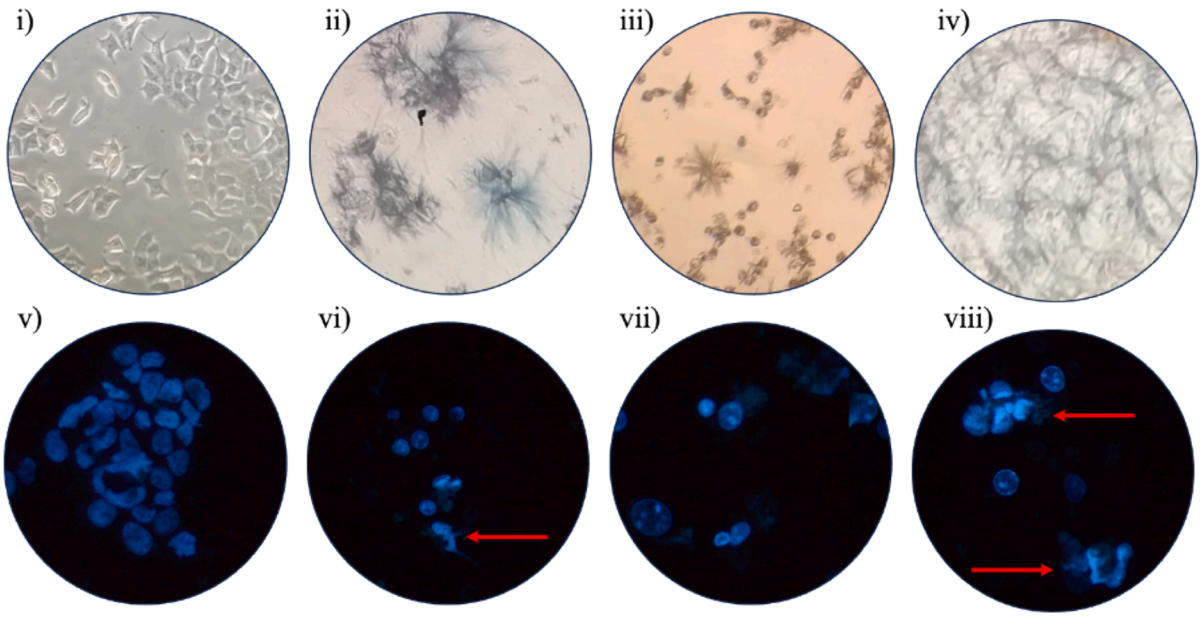

Fig. 4. A) Zoomed inverted light micrographs (magnification 20X) of MCF-7 cells, i) untreated (control); and treated with ii) free TAM 15 μg/mL); iii) bare Fe_3O_4@SiO_2@Cu NPs (125 μg/mL); and iv) TAM (15 μg/mL) co-administrated with Fe_3O_4@SiO_2@Cu NPs (125 μg/mL). B) Fluorescent microscopy images of MCF-7cells v) untreated; and treated with vi) free TAM (15 μg/mL); vii) bare Fe_3O_4@SiO_2@Cu NPs (125 μg/mL); viii) free TAM (15 μg/mlL) co-administrated with Fe_3O_4@SiO_2@Cu NPs (125 μg/mL).

Coadministration of TAM with the Fe_3O_4@SiO_2@Cu hybrid NPs (125 μg/mL) appears to increase the drug efficiency in the tumoral cells as indicated by the reduction in IC_{50} values [19]; however, in healthy ones the variations are within the experimental uncertainty revealing that the different tumoral and cell cytoplasmatic environment (e.g., more acidic conditions, hypoxia, etc) as well as metabolic activity of tumoral cells have a direct impact in the biological response to the administered combination therapy, being effective in the diseased cells. These results are in fair agreement with those previously obtained, for example, by Nosrati et al. [43], who synthesized L-tyrosine-modified Fe_3O_4 magnetic nanoparticles loaded with TAM and evaluated their anticancer effectiveness. These authors revealed that the NPs significantly enhanced the cytotoxic effect of the chemodrug on MCF-7 cells. Similarly, Ruíz-Baltazar et al. [44] observed that superparamagnetic Fe_3O_4-Ag coated nanoparticles significantly lowered the viability of MCF-7 cells but not of human fibroblasts (HFF-1) as in the present case, therefore underscoring the potential therapeutic activity of the NPs themselves in the treatment of BC.

On the other hand, qt-PCR experiments were performed to analyze potential changes in the expression levels of *p53, MDM2* and *MDM4* upon combination treatment. As commented previously, p53 is a transcription factor that controls the activity of genes related to tumor development and growth, and trigger diverse cellular outcomes as programmed cell death, cell division, and DNA damage repair [45]. Downregulation of the *p53* tumor suppressor gene and alterations of its related signaling cascade involving other genes (*TP53*, *MDM2*, *MDM4*, *CDKN2A*, *CDKN2B*, and *TP53BP1*) may reduce apoptosis and promote tumor development [65]. In this regard, elevated expression levels of *MDM2* and *MDM4* have been particularly related to the occurrence of BC [11], and the whole *MDM* family directly influences the dynamic inhibition of the critical tumor suppressor *p53*.

We here observed that co-administering TAM with Fe_3O_4@SiO_2@Cu hybrid NPs resulted in elevated *p53* gene expression in MCF-7 cancer cells (1.8 times) compared to TAM alone. Remarkably, our findings are consistent with the research conducted by Haupt et al. [11], which showed that elevated expression levels of *MDM2* and *MDM4* have been related to the incidence of breast cancer. Interestingly, when TAM and Fe_3O_4@SiO_2@Cu NPs were co-administrated, the *MDM2* and *MDM4* gene expressions were 2.6 and 2.9 times lower compared to TAM free alone in MCF-7 cancer cells. The findings of our study represent the initial evidence indicating that the co-administration of TAM and Fe_3O_4@SiO_2@Cu hybrid NPs resulted in the activation of *p53* as well as in a decrease in *MDM2* and *MDM4*, being correlated with enhanced cytoxicity and cell cell apoptosis in MCF-7 cells. Therefore, the expression levels of *MDM2*, *MDM4*, and *p53* genes might be initially considered as potential biomarkers for assessing both the potential sensitivity to the selected treatment as well as to calibrate the therapeutic outcomes on BC cells, as in the case of the present Fe_3O_4@SiO_2@Cu hybrid NPs and TAM [14]. That is, reinstating *p53* functionality or suppressing *MDM2/MDM4* levels might enhance the cytotoxic efficacy of chemotherapy, as evidenced by numerous preclinical and clinical data [46]. Nevertheless, further experiments would be needed to completely corroborate this hypothesis.

To additionally examine whether TAM coadministration with Fe_3O_4@SiO_2@Cu NPs stimulated apoptosis, MCF-7 cancer cells were stained with Hoechst 33342. Hoechst 33,342 is a fluorescent dye that especially intercalates with nucleic acids in nuclei. Our light microscopy imaged indicated that after 24 h of free TAM coadministration with Fe_3O_4@SiO_2@Cu NPs, morphological alterations (many cells with irregularly shaped masses and reduced cell density) and the presence of fragmented and condensed nuclei were observed under fluorescent microscopy, being such changes much more important if compared to those observed after the administration of only free TAM. These data additionally confirm that tumoral MCF-7 cells initiated cell death by means of apoptosis pathway.

In summary, our results showed that Fe_3O_4@SiO_2@Cu hybrid NPs have great promise as an efficient adjuvant upon coadministration with TAM, and further research is needed in order to perfectly elucidated the whole involved mechanisms of action and their complementarity as well as the evaluation of their pharmacokinetics, biodistribution, and long-term safety, for which the analysis of the present combination therapy in more complex *in vitro* (e.g. 3D tumoral spheroids), and *in vivo* models would be of great value.

5. Conclusions

The present investigation aimed to improve the chemotherapeutic efficacy of TAM by incorporating it with co-administration with Fe_3O_4@SiO_2@Cu NPs, thereby creating a novel and minimally invasive TAM nano-delivery system for the treatment of malignant human breast cancer cells (MCF-7). Initially, it was observed that the average hydrodynamic particle diameter of Fe_3O_4@SiO_2@Cu NPs was approximately ca. 80 nm and exhibited colloidal stability over extended incubation. The results of our *in vitro* cytotoxicity analysis indicate that the therapeutic efficacy of TAM co-administrated with Fe_3O_4@SiO_2@Cu NPs is comparable to that of the free drug at lower concentrations. According to the results of our investigation, administration of 125 μg/mL Fe_3O_4@SiO_2@Cu NPs resulted in a significant reduction of IC_{50} of TAM from 15.4 to 7.8 μg/mL after 72 h of incubation, which was notably lower than the reduction observed after the administration of the free drug. TAM co-administrated with Fe_3O_4@SiO_2@Cu NPs were found to induce a noteworthy increase in apoptosis via *p53*, *MDM2*, and *MDM4* dependent pathways, as well as cytoskeletal structure disruptions, in MCF-7 cancer cells. Overall, the current findings demonstrated the enhanced antiproliferative activity of TAM co-administrated with Fe_3O_4@SiO_2@Cu NPs on MCF-7 cancer cells, as well as their potential as a novel drug adjuvant vehicle to improve the therapeutic efficiency of first-line TAM administration in the treatment of breast cancer.

CRediT authorship contribution statement

Sadegh Salimi: Validation, Methodology, Investigation, Formal analysis, Data curation. **Gholamreza Motalleb:** Writing – review & editing, Writing – original draft, Validation, Supervision, Methodology, Formal analysis, Data curation, Conceptualization. **Hossein Dehghani:** Writing – review & editing, Validation, Supervision, Methodology, Formal analysis, Data curation. **Abbas Rahdar:** Writing – review & editing, Supervision, Conceptualization. **Kazem Dastjerdi:** Validation, Data curation. **Brenda Velasco:** Validation, Investigation, Formal analysis, Data curation. **Pablo Taboada:** Writing – review & editing, Visualization, Funding acquisition, Formal analysis.

Declaration of competing interest

The authors declare that they have no known competing financial interests or personal relationships that could have appeared to influence the work reported in this paper.

Acknowledgements

The Islamic Republic of Iran's University of Zabol and Birjand University of Medical Sciences are highly regarded. The University of Zabol and Birjand University of Medical Sciences accepted this study with the Ethics Committee letter number Ir.bums.REC.1397.376 (1397/12/06). P.T thanks Agencia Estatal de Investigación (AEI) for funding through project PID2022-142682OB-I00 and PCI2022-134981-2, and Xunta de Galicia for grant ED431C 2022/28. ERDF funds are also acknowledged.

Data availability

Data will be made available on request.

References

[1] M. Golshan Ara, G. Motalleb, B. Velasco, A. Rahdar, P. Taboada, Antineoplastic effect of paclitaxel-loaded polymeric nanocapsules on malignant human ovarian carcinoma cells (SKOV-3), J. Mol. Liq. 384 (2023) 122190, https://doi.org/10.1016/j.molliq.2023.122190.

[2] S. Łukasiewicz, M. Czeczelewski, A. Forma, J. Baj, R. Sitarz, A. Stanisławek, Breast cancer-epidemiology, risk factors, classification, prognostic markers, and current treatment strategies-an updated review, Cancers 13 (2021) 4287, https://doi.org/10.3390/cancers13174287.

[3] L. Binkhorst, T. van Gelder, R.H.J. Mathijssen, Individualization of tamoxifen treatment for breast carcinoma, Clin. Pharmacol. Ther. 92 (2012) 431–433, https://doi.org/10.1038/clpt.2012.94.

[4] C. Perou, T. Sørlie, M. Eisen, Molecular portraits of human breast tumours, Nature 406 (2000) 747–752, https://doi.org/10.1038/35021093.

[5] R. Pokhriyal, R. Hariprasad, L. Kumar, G. Hariprasad, Chemotherapy resistance in advanced ovarian cancer patients, Biomark. Cancer. 11 (2019) 1179299X19860815, https://doi.org/10.1177/1179299X19860815.

[6] B. Gao, F. Yang, W. Chen, R. Li, X. Hu, Y. Liang, D. Li, Multidrug resistance affects the prognosis of primary epithelial ovarian cancer, Oncol. Lett. 18 (2019) 4262–4269, https://doi.org/10.3892/ol.2019.10745.

[7] M.M. Gottesman, Mechanisms of cancer drug resistance, Ann. Rev. Med. 53 (2002) 615–627, https://doi.org/10.1146/annurev.med.53.082901.103929.

[8] M.P. Rushika, B. Nabeel, On oncogenes and tumor suppressor genes in the mammary gland, Cold Spring Harb. Perspect. Biol. 4 (2012) a013466, https://doi.org/10.1101/cshperspect.a013466.

[9] M. Gasco, S. Shami, T. Crook, The p53 pathway in breast cancer, Breast Cancer Res. 4 (2002) 1–7, https://doi.org/10.1186/bcr426.

[10] A. Bartnykaitė, A. Savukaitytė, R. Ugenskienė, M. Daukšaitė, E. Korobeinikova, J. Gudaitienė, E. Juozaitytė, Associations of MDM2 and MDM4 polymorphisms with early-stage breast cancer, J. Clin. Med. 10 (2021) 866, https://doi.org/10.3390/jcm10040866.

[11] S. Haupt, R. Vijayakumaran, P.J. Miranda, A. Burgess, E. Lim, Y. Haupt, The role of MDM2 and MDM4 in breast cancer development and prevention, J. Mol. Cell Biol. 9 (2017) 53–61, https://doi.org/10.1093/jmcb/mjx007.

[12] C. Gao, G. Xiao, A. Piersigilli, J. Gou, O. Ogunwobi, J.A. Bargonetti, Context-dependent roles of MDMX (MDM4) and MDM2 in breast cancer proliferation and circulating tumor cells, Breast Cancer Res. 21 (2019) 5, https://doi.org/10.1186/s13058-018-1094-8.

[13] M. Lazzeroni, D. Serrano, B.L. Dunn, B.M. Heckman-Stoddard, O. Lee, S. Khan, A. Decensi, Oral low dose and topical tamoxifen for breast cancer prevention: modern approaches for an old drug, Breast Cancer Res. 14 (2012) 214, https://doi.org/10.1186/bcr3233.

[14] C.M. Day, S.M. Hickey, Y. Song, S.E. Plush, S. Garg, Novel tamoxifen nanoformulations for improving breast cancer treatment: Old wine in new bottles, Molecules 25 (2020) 1182, https://doi.org/10.3390/molecules25051182.

[15] Z. Keramati, G. Motalleb, A. Rahdar, M.A. Kerachian. Anticancer effect of fluorouracil and gum-based cerium oxide nanoparticles on human malignant colon carcinoma cell line (Caco2). Cell J. 25 (2023) 194–202. 10.22074/cellj.2023.562683.1135.

[16] J. Park, S. Thomas, A.Y. Zhong, A.R. Wolfe, G. Krings, M. Terranova-Barberio, N. Pawlowska, L.Z. Benet, P.N. Munster, Local delivery of hormonal therapy with silastic tubing for prevention and treatment of breast cancer, Sci. Rep. 8 (2018) 92, https://doi.org/10.1038/s41598-017-18436-1.

[17] A. Bhatia, R. Kumar, O.P. Katare, Tamoxifen in topical liposomes: development, characterization and in-vitro evaluation, J. Pharm. Sci. 7 (2004) 252–259.

[18] S. Tsymbal, G. Li, N. Agadzhanian, Y. Sun, J. Zhang, M. Dukhinova, V. Fedorov, M. Shevtsov, Recent advances in copper-based organic complexes and nanoparticles for tumor theranostics, Molecules 27 (2022) 7066, https://doi.org/10.3390/molecules27207066.

[19] Y. Gilad, G. Gellerman, D.M. Lonard, B.W. O'Malley, Drug combination in cancer treatment-From cocktails to conjugated combinations, Cancers 13 (2021) 669, https://doi.org/10.3390/cancers13040669.

[20] P. Jaaks, E.A. Coker, D.J. Vis, O. Edwards, E.F. Carpenter, S.M. Leto, et al., Effective drug combinations in breast, colon and pancreatic cancer cells, Nature 603 (2022) 166–173, https://doi.org/10.1038/s41586-022-04437-2.

[21] L.E. van Vlerken, Z. Duan, M.V. Seiden, M.M. Amiji, Modulation of intracellular ceramide using polymeric nanoparticles to overcome multidrug resistance in cancer, Can. Res. 67 (2007) 4843–4850, https://doi.org/10.1158/0008-5472.CAN-06-1648.

[22] D. Deshpande, H. Devalapally, M. Amiji, Enhancement in anti-proliferative effects of paclitaxel in aortic smooth muscle cells upon co-administration with ceramide using biodegradable polymeric nanoparticles, Pharm. Res. 25 (2008) 1936–1947, https://doi.org/10.1007/s11095-008-9614-3.

[23] T. Stack, Y. Liu, M. Frey, S. Bobbala, M. Vincent, E. Scott, Enhancing subcutaneous injection and target tissue accumulation of nanoparticles via co-administration with macropinocytosis inhibitory nanoparticles (MiNP), Nanoscale Horiz. 6 (2021) 393–400, https://doi.org/10.1039/d0nh00679c.

[24] Z. Sun, W. Li, J.C. Lenzo, J.A. Holden, M.J. McCullough, A.J. O'Connor, N. M. O'Brien-Simpson, The potential of calcium phosphate nanoparticles as adjuvants and vaccine delivery vehicles, Front. Mater. 8 (2021) 788373, https://doi.org/10.3389/fmats.2021.788373.

[25] B. Filipić, I. Pantelić, I. Nikolić, D. Majhen, Z. Stojić-Vukanić, S. Savić, D. Krajišnik, Nanoparticle-based adjuvants and delivery systems for modern vaccines, Vaccines 11 (2023) 1172, https://doi.org/10.3390/vaccines11071172.

[26] M. Jeon, M.V. Halbert, Z.R. Stephen, M. Zhang, Iron oxide nanoparticles as T1 contrast agents for magnetic resonance imaging: Fundamentals, challenges, applications, and prospectives, Adv. Mater. 33 (2021) 1906539, https://doi.org/10.1002/adma.201906539.

[27] M. Mahdi Eshaghi, et al., Novel carboxymethyl cellulose-based hydrogel with core–shell Fe_3O_4@ SiO_2 nanoparticles for quercetin delivery, Materials 15 (24) (2022) 8711.

[28] Z.S. Mohammadi, et al., pH-sensitive polyacrylic acid/Fe_3O_4@ SiO_2 hydrogel nanocomposite modified with agarose for controlled release of quercetin, Inorg. Chem. Commun. 163 (2024) 112338.
[29] R. Eivazzadeh-Keihan, F. Radinekiyan, A. Maleki, M. Salimi Bani, Z. Hajizadeh, S. Asgharnasl, A novel biocompatible core-shell magnetic nanocomposite based on cross-linked chitosan hydrogels for *in vitro* hyperthermia of cancer therapy, Int. J. Biol. Macromol. 140 (2019) 407–414, https://doi.org/10.1016/j.ijbiomac.2019.08.031.
[30] L. Fernández, J. González-Rodríguez, M. Gamallo, Z. Vargas-Osorio, C. Vázquez-Vázquez, Y. Piñeiro, J. Rivas, G. Feijoo, M.T. Moreira, Iron oxide-mediated photo-Fenton catalysis in the inactivation of enteric bacteria present in wastewater effluents at neutral pH, Environ. Pollut. 266 (2020) 115181, https://doi.org/10.1016/j.envpol.2020.115181.
[31] K.M. Madhavi, J.R. Ansari, V. Kumar, S. Nagar, A. Sharma, Fe_3O_4 coated SiO_2 magnetic nanoparticles for enhanced antibacterial activity and electrochemical sensing, Metals. 12 (2022) 2145, https://doi.org/10.3390/met12122145.
[32] M.J. Woźniak-Budych, K. Staszak, M. Staszak, Copper and copper-based nanoparticles in medicine-perspectives and challenges, Molecules 28 (2023) 6687, https://doi.org/10.3390/molecules28186687.
[33] R. Eisavi, F. Ahmadi, Fe_3O_4@SiO_2-PMA-Cu magnetic nanoparticles as a novel catalyst for green synthesis of β-thiol-1,4-disubstituted-1,2,3-triazoles, Sci. Rep. 12 (2022) 11939, https://doi.org/10.1038/s41598-022-15980-3.
[34] A. Gao, H. Liu, L. Hu, H. Zhang, A. Hou, K. Xie, Synthesis of Fe_3O_4@SiO_2-Au/Cu magnetic nanoparticles and its efficient catalytic performance for the Ullmann coupling reaction of bromamine acid, Chinse Chem. Lett. 29 (2018) 1301–1314, https://doi.org/10.1016/j.cclet.2017.11.040.
[35] C.D. Helgason, C.L. Miller, Basic Cell Culture Protocols, 3rd ed., Humana Press, 2004.
[36] S.M. Taimoory, A. Rhadar, M. Aliahmad, F. Sadeghfar, M.R. Hainezhad, The synthesis and characterization of a magnetite nanoparticle with potent antibacterial activity and low mammalian toxicity, J. Mol. Liq. 265 (2018) 96–104, https://doi.org/10.1016/j.molliq.2018.05.105.
[37] M. Darroudi, M.B. Taj. Facile synthesis of Fe3O4/SiO2/Cu nanoparticles: investigation of physicochemical attributes of interaction in cationic micellar media and photo-antibacterial impact. Dig. J. Nanomater. Bios. 2 (2022) 607-622. 10.15251/djnb.2022.172.607.
[38] A.Y. Ziganshina, E.E. Mansurova, A.D. Voloshina, A.P. Lyubina, S.K. Amerhanova, M.M. Shulaeva, I.R. Nizameev, M.K. Kadirov, L.R. Bakhtiozina, V.E. Semenov, I. S. Antipin, Thymine-modified nanocarrier for doxorubicin delivery in glioblastoma cells, Molecules 28 (2023) 551, https://doi.org/10.3390/molecules28020551.
[39] L.G. Arellano, E.M. Villar-Alvarez, B. Velasco, V. Dominguez-Arca, G. Prieto, A. Cambón, S. Barbosa, P. Taboada, Light excitation of gold Nanorod-Based hybrid nanoplatforms for simultaneous bimodal phototherapy, J. Mol. Liq. 377 (2023) 121511, https://doi.org/10.1016/j.molliq.2023.121511.
[40] B.I. Macías-Martínez, D.A. Cortés-Hernández, A. Zugasti-Cruz, B.R. Cruz-Ortíz, E. M. Múzquiz-Ramos, Heating ability and hemolysis test of magnetite nanoparticles obtained by a simple co-precipitation method, J. Appl. Res. Technol. 14 (2016) 239–244, https://doi.org/10.1016/j.jart.2016.05.007.
[41] H. Tabasi, M.T. Hamed Mosavian, Z. Sabouri, M. Khazaei, M. Darroudi, pH-responsive and CD44-targeting by Fe_3O_4/MSNs-NH_2 nanocarriers for oxaliplatin loading and colon cancer treatment, Inorg. Chem. Commun. 125 (2021) 108430, https://doi.org/10.1016/j.inoche.2020.10843011.
[42] S. Taghavi, M. Shahnani, H. Rafati. Preparation and characterization of tamoxifen loaded silica and NH2 functionalized mesoporous silica nanoparticles as delivery systems against MCF-7 breast cancer cells. Iran J. Basic. Med. Sci. 26 (2023) 1334-1341. 10.22038/IJBMS.2023.70152.15254.
[43] H. Nosrati, N. Rashidi, H. Danafar, et al., Anticancer activity of tamoxifen loaded tyrosine decorated biocompatible Fe_3O_4 magnetic nanoparticles against breast cancer cell lines, J. Inorg. Organomet. Polym. 28 (2018) 1178–1186, https://doi.org/10.1007/s10904-017-0758-7.
[44] Á.D.J. Ruíz-Baltazar, S.Y. Reyes-López, N. Méndez-Lozano, K. Juárez-Moreno, Evaluation of superparamagnetic Fe_3O_4-Ag decorated nanoparticles: cytotoxicity studies in human fibroblasts (HFF-1) and breast cancer cells (MCF-7), Appl. Sci. 14 (2024) 6750, https://doi.org/10.3390/app14156750.
[45] L. Carlsen, S. Zhang, X. Tian, A. De La Cruz, A. George, T.E. Arnoff, W.S. El-Deiry, The role of p53 in anti-tumor immunity and response to immunotherapy, Front. Mol. Biosci. 10 (2023) 1148389, https://doi.org/10.3389/fmolb.2023.1148389.
[46] K.T. Bieging, S.S. Mello, L.D. Attardi, Unravelling mechanisms of p53-mediated tumour suppression, Nat. Rev. Cancer 14 (2014) 359–370, https://doi.org/10.1038/nrc3711.